Molecular Therapy
Methods & Clinical Development
Original Article

A C1qTNF3 collagen domain fusion chaperones diverse secreted proteins and anti-Aβ scFvs: Applications for gene therapies

Brenda D. Moore,[1,2,3,4,6] Yong Ran,[1,2,3,4,6] Marshall S. Goodwin,[3,4] Kavitha Komatineni,[3,4] Karen N. McFarland,[4,5,6] Kristy Dillon,[3,4] Caleb Charles,[3,4] Danny Ryu,[1,2,3,4,6] Xuefei Liu,[1,2,3,4,6] Stefan Prokop,[4,6,7] Benoit I. Giasson,[3,4,6] Todd E. Golde,[1,2,3,4,6] and Yona Levites[1,2,3,4,6]

[1]Department of Pharmacology and Chemical Biology, Emory University School of Medicine, Atlanta, GA, USA; [2]Center for Neurodegenerative Disease, Emory University, School of Medicine, Atlanta, GA, USA; [3]Department of Neuroscience, University of Florida College of Medicine, Gainesville, FL, USA; [4]Center for Translational Research in Neurodegenerative Disease, College of Medicine, University of Florida, Gainesville, FL, USA; [5]Department of Neurology, University of Florida College of Medicine, Gainesville, FL, USA; [6]McKnight Brain Institute, University of Florida College of Medicine, Gainesville, FL, USA; [7]Department of Pathology, University of Florida, Gainesville, FL, USA

Enhancing production of protein cargoes delivered by gene therapies can improve efficacy by reducing the amount of vector or simply increasing transgene expression levels. We explored the utility of a 126-amino acid collagen domain (CD) derived from the C1qTNF3 protein as a fusion partner to chaperone secreted proteins, extracellular "decoy receptor" domains, and single-chain variable fragments (scFvs). Fusions to the CD domain result in multimerization and enhanced levels of secretion of numerous fusion proteins while maintaining functionality. Efficient creation of bifunctional proteins using the CD domain is also demonstrated. Recombinant adeno-associated viral vector delivery of the CD with a signal peptide resulted in high-level expression with minimal biological impact as assessed by whole-brain transcriptomics. As a proof-of-concept *in vivo* study, we evaluated three different anti-amyloid Aβ scFvs (anti-Aβ scFvs), alone or expressed as CD fusions, following viral delivery to neonatal CRND8 mice. The CD fusion increased half-life, expression levels, and improved efficacy for amyloid lowering of a weaker binding anti-Aβ scFv. These studies validate the potential utility of this small CD as a fusion partner for secretory cargoes delivered by gene therapy and demonstrate that it is feasible to use this CD fusion to create biotherapeutic molecules with enhanced avidity or bifunctionality.

INTRODUCTION

Multiple factors can limit the potential efficacy of a gene therapy. Despite recent clinical successes, many challenges still limit most gene therapy approaches.[1–6] To date, most efforts to optimize gene therapies have focused on optimizing the vector for delivery to target cells with a major emphasis on maximizing distribution and expression of the transgene. Such studies have enabled advances with respect to capsid engineering, selection of promoters, and vector sequence optimization.[7] Much less attention has been paid to the optimization of the encoded biotherapeutic protein. Because the efficacy of gene therapies that deliver protein cargoes will, in most cases, be linked to the overall biological activity and expression level of the encoded transgene, efforts to optimize the activity, expression, and stability of the protein produced from the encoded transgene should be explored.

Much of our own work using recombinant adeno-associated viral vectors (rAAV) has focused on the delivery of protein cargoes intended to act in a non–cell-autonomous fashion to the brains of preclinical models of Alzheimer disease (AD)–relevant pathologies.[8–12] Especially when considering a potentially translational program designed to deliver a biotherapeutic to the brain, except in rare circumstances, it is very difficult to transduce enough cells to provide a therapeutic effect if the encoded transgene only functions in a cell-autonomous fashion. Furthermore, both within the brain and in the periphery, there are opportunities to use rAAV vectors to deliver transgenes encoding secretory proteins that can be therapeutic. Delivery within the brain bypasses the issues of blood-brain barrier penetrance and can result in widespread distribution of the secreted protein. In the periphery, more focal delivery of a secreted biotherapeutic (e.g., to a solid tumor or tumor microenvironment) could provide local target engagement yet avoid more systemic toxicities and thereby increase the therapeutic index.

Received 22 May 2023; accepted 26 October 2023;
https://doi.org/10.1016/j.omtm.2023.101146.

Correspondence: Brenda D. Moore, Department of Pharmacology and Chemical Biology, Emory University School of Medicine, Atlanta, GA, USA.
E-mail: brenda.dawn.moore@emory.edu
Correspondence: Yona Levites, Department of Pharmacology and Chemical Biology, Emory University School of Medicine, Atlanta, GA, USA.
E-mail: yona.levites@emory.edu

With a focus on using rAAVs to deliver secreted biotherapeutics, we set out to identify a domain that could enhance secretion, avidity, and stability of a fusion partner. Desired properties for this domain included (1) small size, so that it would have minimal impact on the size of the biotherapeutic protein that could be encoded within the packing limit of the vector; (2) no known biological effector function; and (3) be derived from an endogenous mammalian protein and therefore less likely to be immunogenic. We hypothesized that the relatively small collagen domains (CDs) derived from the complement C1q tumor necrosis factor–related protein 3 (C1qTNF) protein family members (C1qTNF3 and -5), that are expressed at very low levels in the brain and show restricted tissue expression in the periphery, may serve to multimerize, stabilize, and enhance the secretion of various protein biotherapeutics. Here, we show that a small 126-amino acid (aa) CD, based on the CD domain found in C1qTNF3, has many of the desired properties and, when fused to numerous proteins, it enhances secretion while maintaining (or amplifying) the functionality of the fusion partner. The flexibility of this domain is further shown through the facile development of bifunctional molecules using the CD domain that target both amyloid-β (Aβ) and tau. Intraperitoneal injection of a recombinant single-chain variable antibody fragment (scFv) and its cognate CD fusion showed that the CD modestly extended the half-life of the protein in circulation. rAAV-mediated expression of the CD in amyloid-β precursor protein (APP) CRND8 and nontransgenic mice brains shows robust expression, but no impact on amyloid deposition or brain function as assessed by bulk whole-brain transcriptomics. Finally, as a proof-of-concept impact of expression, we evaluated the effect of three different anti-Aβ scFvs by themselves and when fused to the C1qTNF3 CD on amyloid pathology in APP CRND8 mice and documented improved efficacy of a low-affinity anti-Aβ scFv when it was fused to the CD.

RESULTS

A 126-aa CD from C1qTNF3 enhances secretion and multimerization of recombinant proteins

Our laboratory has a broad interest in biotherapeutics based on recombinant antibody fragments, immune decoy receptors derived from extracellular domains of type I and type II membrane proteins, and other secreted proteins that could influence immune function and AD pathologies.[8,11–14] However, we have observed that despite efficient transduction, inefficient expression of select scFvs and immune decoy receptors may limit therapeutic efficacy in the context of preclinical studies of rAAV-mediated gene therapies. Therefore, we evaluated whether CDs derived from C1qTNF proteins could enhance protein expression and secretion. For our initial studies, we focused on the extracellular domain of the immune checkpoint protein Ctla4, fused at the N-terminus to a 63-aa CD (1xCD) and a 126-aa CD (2xCD) derived from C1qTNF3 (Figure 1A, Table S1). As observed in Figure 1B, when comparing 1xCD and 2xCD fusions, addition of the 2xCD resulted in increased expression and apparent dimerization of Ctla4 protein. Thus, our subsequent experiments used the 2xCD fusion, which hereafter will be referred to simply as CD. Two additional immune checkpoint co-inhibitory molecules, lymphocyte activation gene 3 (LAG-3) and programmed cell death protein 1 (PDCD1, PD-1), fused to 2xCD, were detected at much higher levels in the media when compared to the non-CD fusions (Figure 1C). We also fused the CD to additional proteins such as sNOTCH1, sDLL3, tissue inhibitor of metalloproteinases 1 (Timp1), and Timp3. As shown in Figure 1C, in all cases the CD fusion resulted in significantly higher levels of secreted protein in the media. C1qTNF family proteins have been shown to trimerize and form higher-order multimerizations. Thus, we assessed the multimerization state of several of our CD fusion proteins. When separated on reducing SDS-PAGE gels, we noted that the CD fusion proteins often migrated as dimers, trimers, or even higher-order assemblies. Thus, for a variety of secreted proteins, fusion to the 126-aa CD results in increased levels of the protein in the media and some degree of multimerization.

To further evaluate the state of multimerization of CD fusion, we performed size exclusion chromatography on the secreted Lag3-CD fusion. Although C1qTNF family members are thought to predominantly form trimers, and collagen domains typically result in trimeric assemblies, the most abundant multimer of Lag3-CD, based on these studies, was a dimer (Figure S1).

We next evaluated the ability of CD fusion to increase the expression and stability of known scFvs that target proteins of therapeutic relevance to AD and Parkinson disease. ScFvs specific to Aβ (scFv9), the fourth microtubule repeat region (4R) of tau (scFv6), phosphorylated (p)tau (scFvPHF1), and human α-synuclein (scFv12) were fused to CD, which resulted in higher levels of expressed protein in the lysate, as well as high levels of secreted protein, a large proportion of which was a dimer, with some trimer and tetramer fractions (Figure 1D). Whereas the expected molecular weight of scFv alone is 30 kDa, scFv-CD is 44 kDa, bands ∼88, 132, and 176 kDa, corresponding to dimers, trimers, and tetramers, were detected on both reducing and nonreducing gels in the media as well as cell lysates. Interestingly, CD alone was detected as a dimer and tetramer in the media as well as a higher molecular order species in the lysate. These scFvs retained their antigen binding and specificity when subjected to direct ELISA coated with corresponding antigen (Figure 1E), suggesting that CD is an ideal candidate for stabilizing and multimerizing secreted proteins.

Dual fusions of scFvs to the NH_2- and COOH-terminus of the CD result in bifunctional proteins

We next evaluated the feasibility of creating a bifunctional CD fusion protein. We generated a construct consisting of secreted anti-Aβ scFv9, CD, and the anti-tau scFv6 (Figure 2A). This protein was secreted efficiently into the media and was detected as a monomer and dimer on an SDS-PAGE gel (expected molecular weight of this bispecific scFv is ∼70 kDa for a monomer and ∼140 kDa for a dimer) (Figure 2B). The protein retained the functionality of the anti-tau and anti-Aβ scFvs because it bound to plaques and tangles in mouse and human tissues and to recombinant tau and Aβ in ELISAs (Figures 2C and 2D).

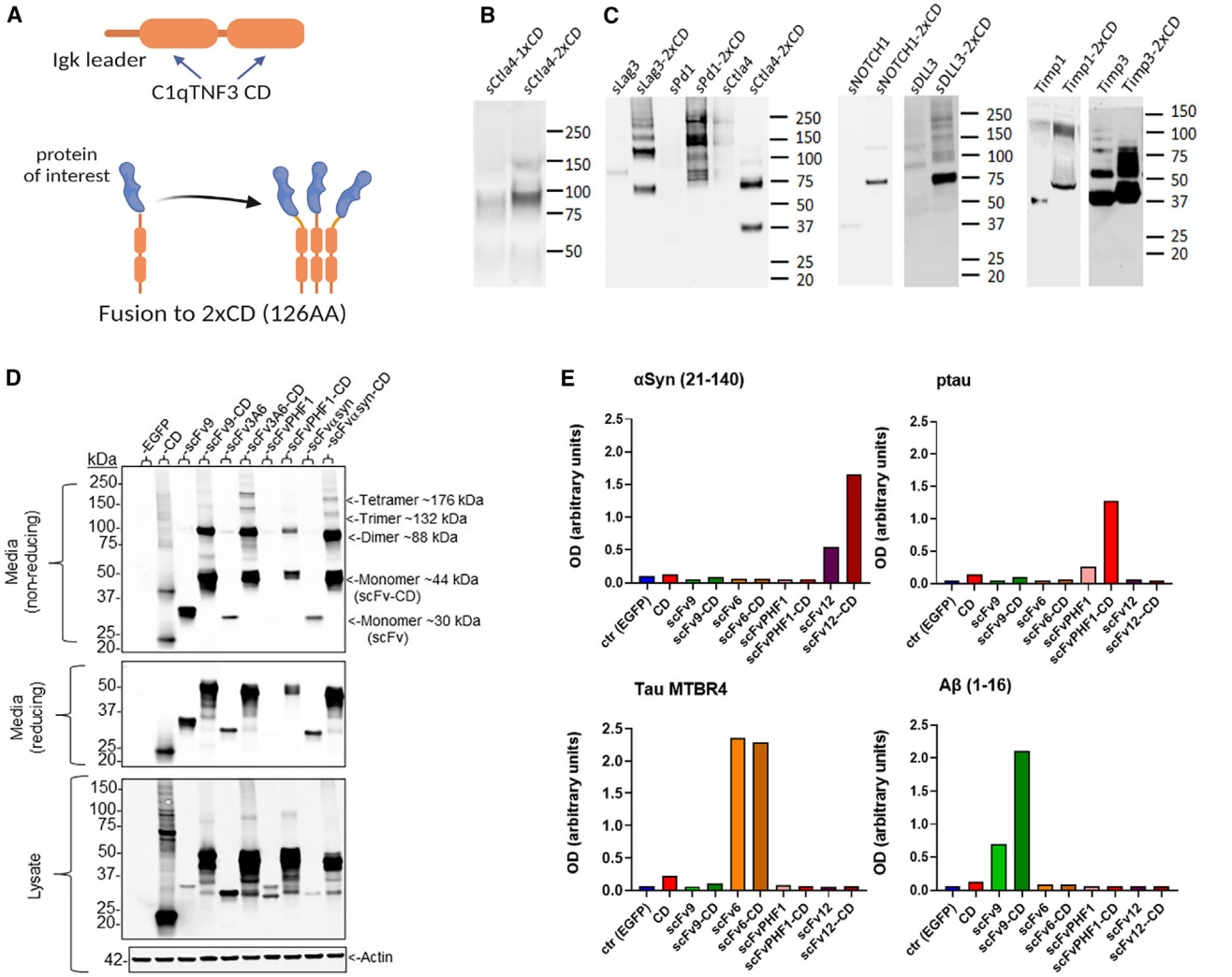

Figure 1. A 126 amino-acid CD from C1qTNF3 enhances secretion and multimerization of recombinant proteins

(A) Schematic of 2xCD under Igkappa secretion leader fused to a protein of interest. A protein of interest fused to 2xCD can readily multimerize. (B and C) Conditioned media from transiently transfected HEK cells were subjected to SDS-PAGE without reducing agent and immunoblotted with FLAG. (B) 1xCD and 2xCD derived from C1qTNF3 were fused to COOH-terminal soluble Ctla4. (MW (Ctla4) = 40kDa, expected MW (CTLA4 - 1xCD) = 52 KdA, MW (CTLA4 - 2xCD+ = 64 kDA). (C) Soluble proteins Lag3, Pd1, Ctla4, NOTCH1, DLL3, Timp1, and Timp3 either alone or fused to 2xCD derived from C1qTNF3. MW (Lag3) = 57kDa, MW (PD1) = 50kDa, MW (N-terminal NOTCH1) = 53kDa, MW (N-terminal DLL3) = 49kDa, MW (Timp1) = 28kDa, MW (Timp3) = 30kDa. (D) Media with and without reducing agent and lysates from cells transfected with plasmids expressing scFv9, scFv6 (against 4R tau), scFvPHF1, or scFv12 (against N-terminal a-syn) with and without CD. EGFP and CD alone are controls, β-actin as a loading control. Cell lysates with reducing agent are also shown. (E) Media from cells expressing scFv9, scFv6 (against 4R tau), scFvPHF1, or scFv12 (against N-terminal a-syn) with and without CD was subjected to direct ELISA coated with a-syn (21–140), ptau, tau MTBR4, and Aβ (1–16). Anti-Flag-HRP antibody was used as detection. n = 2–3 independent experiments.

CD alone has no effect on cognitive function or amyloid plaque burden

To determine whether overexpression of secreted CD by itself influenced cognitive function or amyloid pathology, we delivered rAAV2/1-CD into the cerebral ventricles of newborn TgCRND8 mice (transgenic for human APP K670N, M671L, V717F, and APPswe/ind), These mice show rapid-onset Aβ pathology, with deposits detected as early as 2 months of age. At 6 months, the mice were behaviorally tested in a fear-conditioning paradigm.[15] Control groups included mice injected with PBS. An analysis of contextual and tone recall revealed that CD had no effect on these behaviors in either the TgCRND8 mice or their NTg littermates (Figures 3A and 3B).

Following the behavioral studies, the mice were euthanized, and their brains were harvested for Aβ analysis by immunohistochemistry (IHC). Amyloid burden, assessed by scanning and quantification of brain sections stained with anti-pan-Aβ biotinylated antibody, was

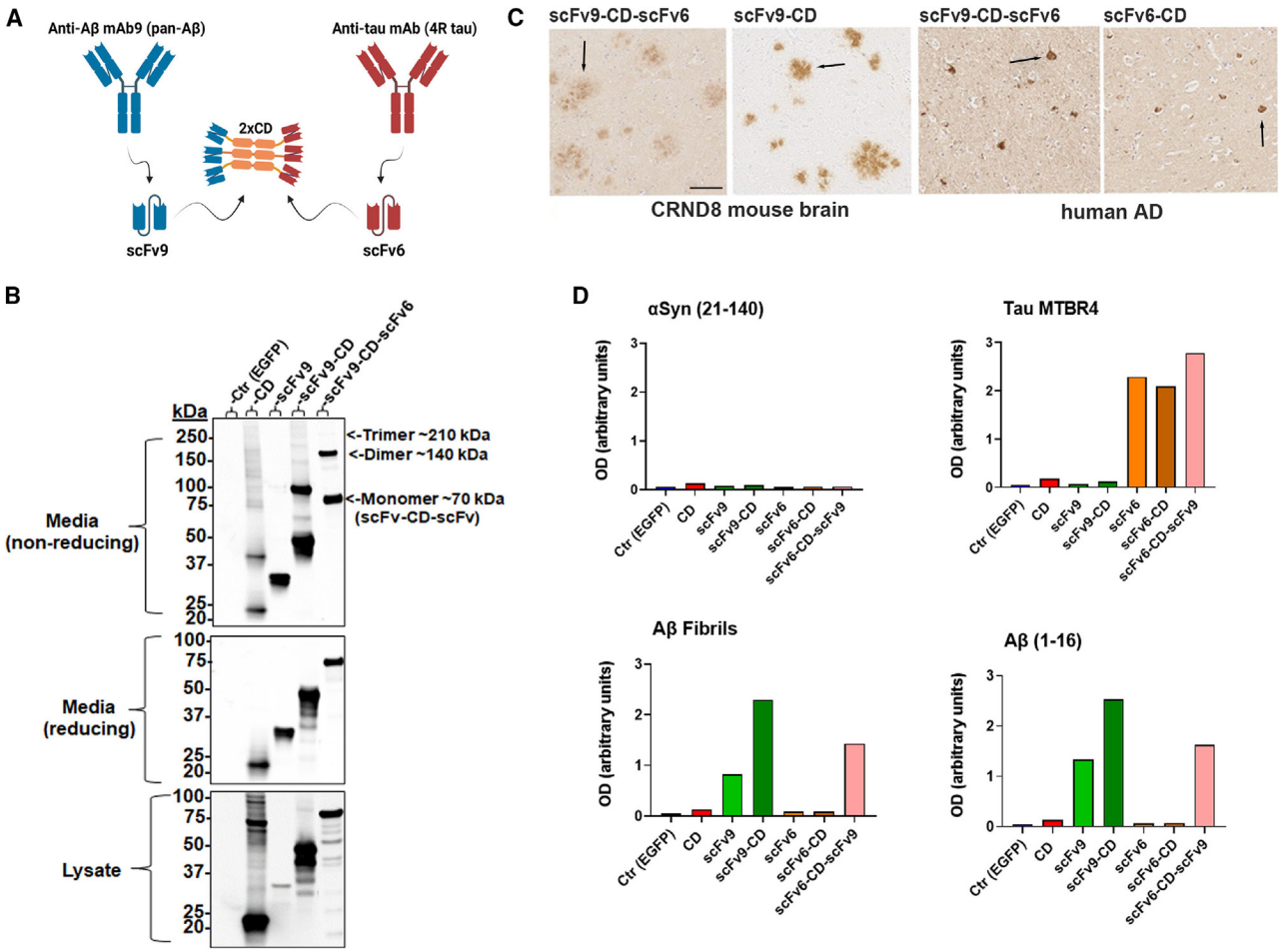

Figure 2. Dual fusions of scFvs to the NH2- and COOH- terminus of the collagen domain result in bifunctional proteins

(A) Schematic of anti-tau/anti-Aβ bispecific scFv construction using scFv9 (specific to pan-Aβ) and scFv6 (specific to tau 4R) fused to CD. (B) Conditioned media from HEK cells transiently expressing scFv9-CD, scFv6-CD, or scFv9-CD-scFv6 was used to visualize amyloid plaque pathology on brain tissue from 6 month old TgCRND8 mice (Aβ plaques) or neurofibrillary tangles on human AD brain (tangles). n = 3 independent experiments, scale bar: 25μm. Arrows point to amyloid plaques in mouse tissue and neurofibrillary tangles on human brain tissue. (C) Lysates and media from cells transfected with plasmids expressing scFv9, scFv6 (against 4R tau), or scFv9-CD-scFv6 were subjected to SDS-PAGE without or with reducing agent and immunoblotted with FLAG. EGFP and CD alone are controls. Cell lysates with reducing agent are also shown. (D) Media was subjected to direct ELISA coated with a-syn (21–140), tau MTBR4, Aβ fibrils and monomeric Aβ (1–16). Anti-Flag-HRP antibody was used as detection. n = 2–3 independent experiments.

not attenuated by the overexpression of CD (Figures 3C and 3D). We also examined and counted cored Aβ plaques by Thioflavin S staining (Figure 3E) and found no difference in Thioflavin S-positive load (Figure 3F).

To identify transcriptional changes in response to CD overexpression, RNA isolated from the hemibrains of mice expressing CD or PBS control was sequenced (Figure 3G). Using cutoff values for an absolute value of 1 for the log2FoldChange and adjusted p value less than 0.05, we identified 1 upregulated gene and 2 downregulated genes. As expected, *C1qtnf3*, the parent gene of CD, was the most significantly upregulated gene (log2FoldChange = 7.35, adjusted p value = 6.67×10^{-61}). Two genes were downregulated, *Tmem267* (log2FoldChange = −1.02, adjusted p value = 4.48×10^{-2}) and a gene involved in immune response, *Ccl28* (log2FoldChange = −3.04, adjusted p value = 1.45×10^{-10}). It is striking that the expression of only 3 genes, or 0.01% of genes, were altered out of a total of 22,046 protein coding genes. This alteration probably can be explained by the statistical probability of changes caused by pure chance.

We then evaluated the effect of CD on Aβ42 aggregation *in vitro*. Under conditions in which synthetic Aβ42 aggregates into Thioflavin T-positive structures, CD had no impact, neither increased nor inhibited aggregation (Figure 3H). These findings suggest that CD alone has no effect on amyloid burden or cognitive functions, supporting the further development of recombinant therapeutics using this fusion for improved stability, expression, and affinity.

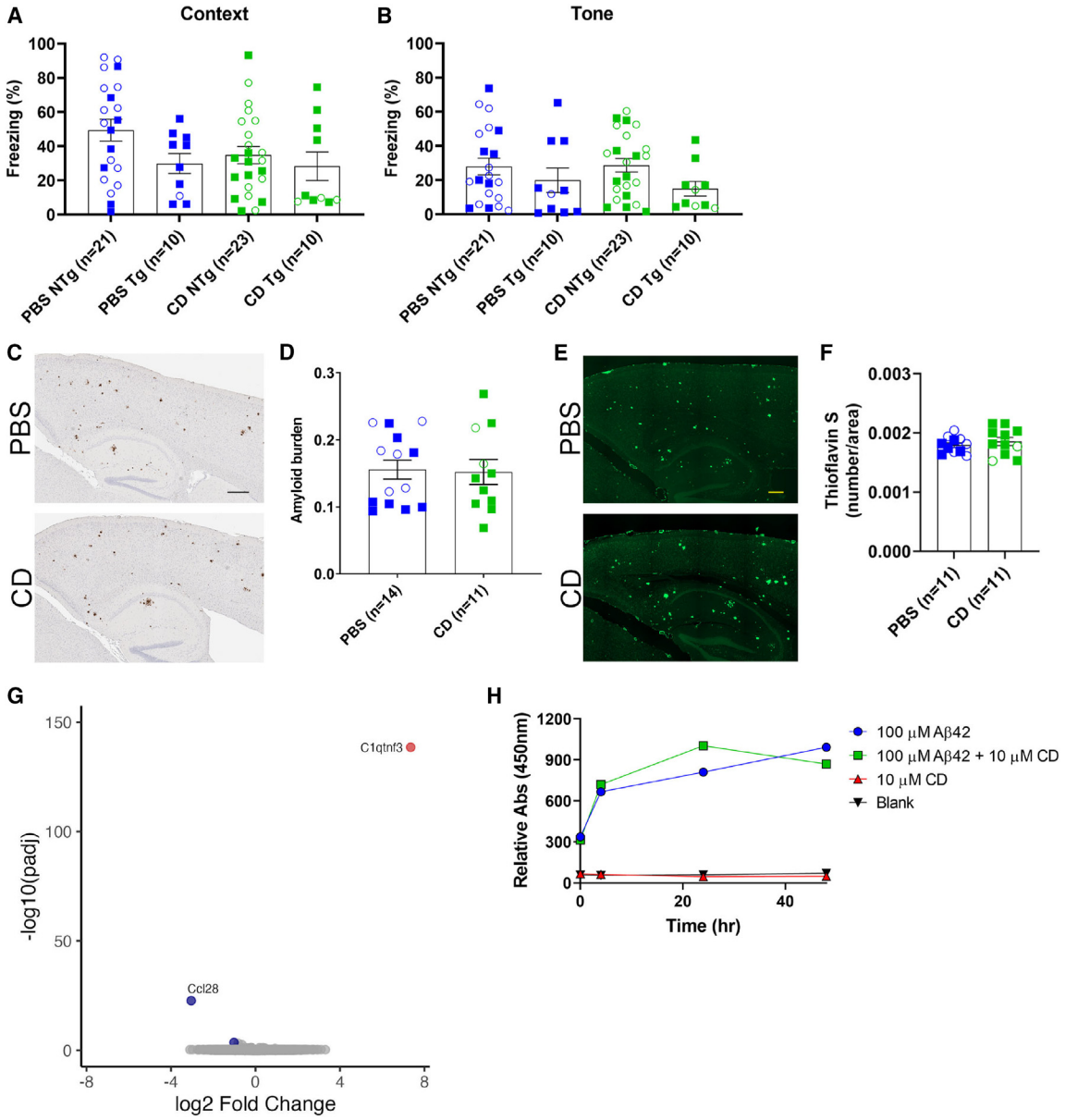

Figure 3. CD alone has no effect on cognitive function or plaque burden

CRND8 mice were intracerebrally injected with rAAV-CD or PBS (control) at P0. (A, B) Mice were subjected to contextual fear conditioning at 6 mo of age. Mean percentage freezing ± standard error of the mean exhibited by TgCRND8 and NTg overexpression of CD or control (PBS). (A) Context paradigm. (B) Tone test. n = 10/Tg, n = 21–23/NTg mice per group. Filled square = male; open circle = female. (C) Representative brain sections (cortex and hippocampus) of TgCRND8 mice overexpressing CD or PBS (control) stained with anti-Aβ mAb 33.1.1-biotin. Scale bar: 250 μm. (D) Quantification of amyloid deposits immunostained with anti-Aβ mAb 33.1.1-biotin. Data represents mean ± standard error of the mean; n = 11–14 mice per group. Filled square = male; open circle = female. (E) Representative brain sections of TgCRND8 mice overexpressing CD or PBS (control) stained with Thio-S. Bar: 200 μm. (F) Quantification of Thio-S plaques per area measured. Data represents mean ± standard error of the mean. n = 11 mice per group. Filled square = male; open circle = female. (G) Volcano plot of differentially expressed genes of mice overexpressing CD versus control. n = 4. (H) Monomeric Aβ1-42 (100 mM) were incubated with CD (10 mM) in buffer (20 mM Tris-HCl, 150 mM NaCl, pH 8.0) with shaking at 37°C. At the indicated times, aliquots were diluted 15-fold for measurement of Thioflavin T fluorescence.

Fusion of CD to anti-Aβ single-chain antibodies results in increased multimerization and binding

To evaluate the effects of CD fusion on anti-Aβ scFvs and their subsequent binding to Aβ, we chose three candidate scFvs: (1) scFv9,[11] (2) an scFvs derived from a novel mouse monoclonal antibodies to Aβ, 2B12 (Figures 4A and 4B), and (3) B11, an scFv derived from the variable regions of aducanumab, which is a high-affinity human immunoglobulin G1 (IgG1) monoclonal antibody (mAb) isolated

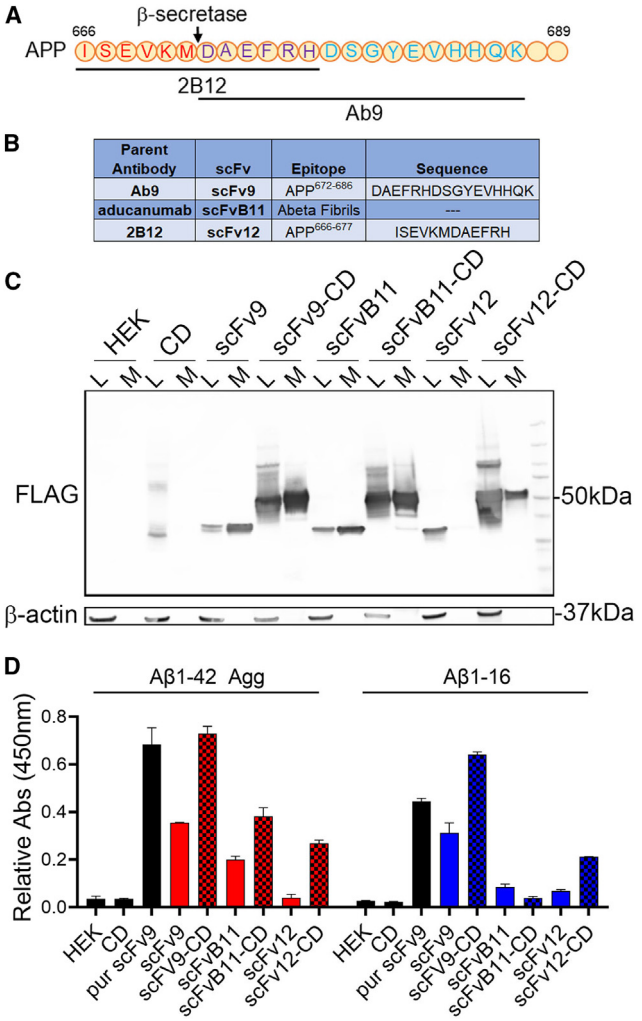

Figure 4. CD fusion to anti-Aβ scFvs results in multimerization, increased stability, and binding of scFvs

(A) Schematic depiction of the antigens used to generate monoclonal antibodies Ab9 (scFv 9) and 2B12 (scFv 12). Ab9 antigen, depicted in purple and blue, is Aβ1-16. The 2B12 antigen, depicted in red and purple, ISEVKMDAEFRH, is a peptide fragment that spans the BACE cleavage site of the amyloid-β precursor protein (APP). (B) scFvs used in this study. (C) Cell lysate (L) and media (M) of HEK cells transfected with scFv9, scFv9-CD, scFvB11, scFvB11-CD, scFv12, scFv12-CD, or CD alone (control), were subjected to SDS-PAGE and immunoblotted with FLAG, β-actin is loading control. (D) Media of HEK cells expressing scFvs, scFvs-CD, or CD alone (control) were subjected to direct ELISA. Plates were coated with either Aβ1-42 aggregates or monomeric Aβ1-16 and scFv binding was detected with anti-c-myc-HRP. Data represents mean ± SEM of three independent transfections.

from human B cells and shown to have a high affinity to aggregated Aβ.[16,17] The mAb 2B12, an IgG2a, was raised against an epitope that spans across the β-secretase cleavage site ($APP^{666-677}$), it preferentially detects N-terminal Aβ peptides, and it immunostains amyloid plaques in multiple APP transgenic mouse models (Figure S2). The 2B12 mAb does not detect N-terminal truncated Aβ peptides or pyroglutamate-Aβ3-42, but it does immunostain amyloid plaques comparable to pan-Aβ antibody (Figure S2). It has a lower affinity to Aβ as compared to mAb9.

scFvs derived from the three antibodies were fused to CD and expressed in HEK293T cells. Immunoblotting of the secreted scFv-CD fusion proteins confirms expression and multimerization; CD fusion resulted in increased levels of scFvs secreted to the media, as compared to control scFvs, as well as SDS-stable higher-molecular-weight species, corresponding to dimers and trimers (Figure 4C). Binding to Aβ was validated by direct ELISA, with either Aβ1-42 aggregates or monomeric Aβ1-16 as the capture. The signal resulting from the binding of media containing scFv alone was compared to the signal from the binding of media with secreted scFv-CD. The secreted scFv-CD showed increased binding signals relative to the scFv alone. The signals for scFv9-CD binding to Aβ1-42 aggregates and Aβ1-16 were increased 2.05-fold and 2.08-fold, for scFvB11-CD were increased 1.91-fold and no effect, and for scFv12-CD were increased 7.79-fold and 3.15-fold, respectively (Figure 4D). scFvB11 and scFvB11-CD weakly interacted with monomeric Aβ1-16, as expected, because the parent antibody was purified based on its binding to Aβ aggregates. In addition, we evaluated the ability of neural cells to secret CD-fused scFv with retained binding ability. Organotypic slice cultures (brain slice cultures) were transduced with scFv9 and scFv9-CD. scFv and scFv-CD were detected in the conditioned media and were able to bind Aβ1-42 aggregates. The levels of scFv9-CD were 2.17-fold higher than scFv9 alone (Figures S3A and S3B). These studies demonstrate that the fusion of CD to multiple anti-Aβ scFvs increases secretion while maintaining the target binding properties of parental scFv.

CD increases expression of scFvs in the brain and extends half-life of scFv9

As a next step, we tested whether CD fusion would attenuate scFv effects on amyloid aggregation *in vivo*. To evaluate expression of the scFv-CD in the brain, scFvs and scFv-CDs were packaged into the rAAV2/1 and injected into newborn TgCRND8 mice. IHC staining of nontransgenic littermates (NTg) shows that all of the scFv-CDs have increased staining in cell bodies compared to their corresponding scFv (Figure 5A). Interestingly, scFvs are expressed evenly through the parenchyma, whereas scFv-CD staining is more concentrated in cell bodies. scFv-CD levels in brain radioimmunoprecipitation assay (RIPA) extracts bound to Aβ1-42 aggregates are 2.42-fold higher than scFv alone (Figures S3C and S3D). In addition, we examined the effect of CD fusion on scFv half-life *in vivo*; equal amounts of scFv9-CD or scFv9 (250 μg) were administered to mice by intraperitoneal (IP) injection, and plasma scFv levels were measured at 0, 2, 4, 8, and 24 h after injection (Figure 5B). Plasma levels of scFv9-CD were increased at all of the time points compared to scFv9 control, resulting in an ∼2.5-fold extension of scFv9 half-life, 1.82 h compared to 0.74 h, respectively (Figure 5B).

Proof of concept *in vivo* study of scFv-CD effects on amyloid formation

Next, we explored whether CD fusion to anti-Aβ scFvs improves scFv-mediated attenuation of amyloid aggregation. We delivered

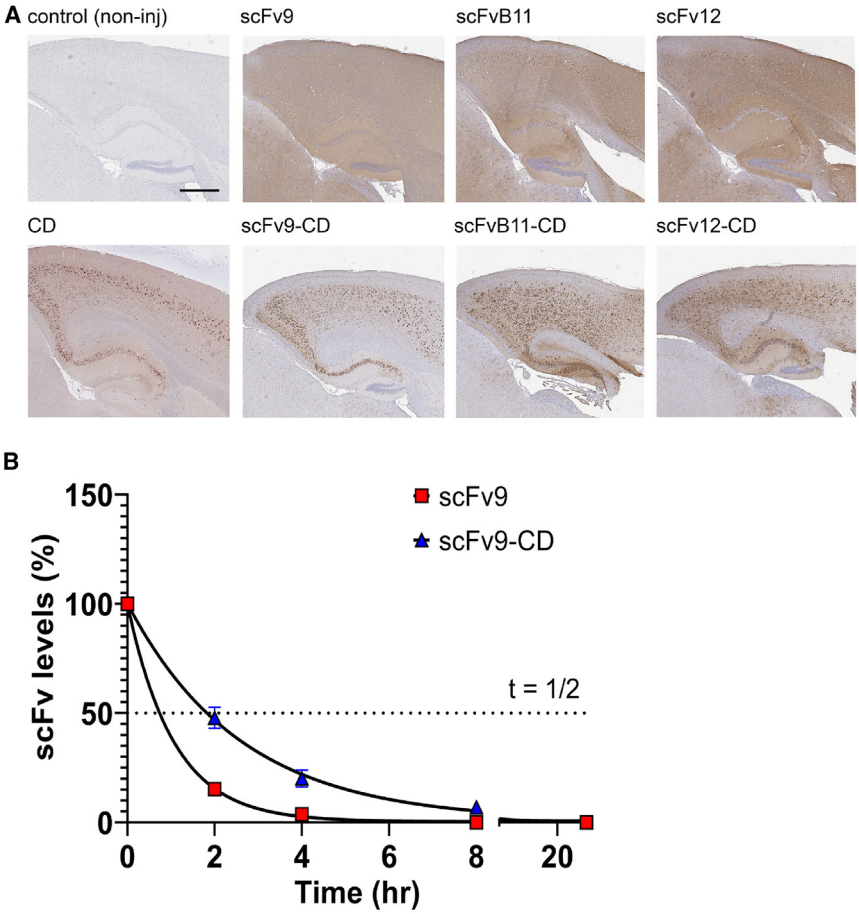

Figure 5. CD increases expression of scFvs in the brain and improves the half-life of scFv9

(A) P0 CRND8 mice were intracerebrally injected with rAAV-scFv9, scFv9-CD, scFvB11, scFvB11-CD, scFv12, scFv12-CD, PBS, or CD. Representative brain sections (hemi-brain) of NTgCRND8 mice stained with anti-FLAG mAb. Scale bar: 250 μm. (B) Plasma scFv levels from female B6C3F1 mice injected with biotinylated scFv9 or scFv9-CD (250 μg) collected at the indicated times. Data presented as mean ± standard error of the mean, n = 4.

rAAV2/1-scFv9, scFv9-CD, scFvB11, scFvB11-CD, scFv12, and scFv12-CD to the brains of newborn TgCRND8 mice. Noninjected mice were used as controls. Amyloid deposition in the cortex and hippocampus of these mice was examined by IHC with a pan-Aβ antibody in the 3-month-old mice. At this age, TgCRND8 mice have limited pathology, presenting as a small number of plaques in the cortex and hippocampus and low but detectable levels of SDS-insoluble, formic acid (FA)-soluble Aβ[11,12] (Figures 6A and 6B). Furthermore, we assessed levels of soluble and insoluble Aβ in the brains of TgCRND8 mice treated with scFvs and scFvs-CD. A series of sequential extractions were performed and Aβ40 and Aβ42 levels were measured by ELISA using C-terminal-specific antibodies. The detection limit of the ELISA is 0.04 pmol/g (Figure 7). Concomitantly, with our previous findings,[11] scFv9 significantly reduced amyloid deposition; however, fusion of CD to scFv9 did not augment the ability of scFv9 to prevent amyloid aggregation because there was no difference in the number of amyloid plaques between scFv9 and scFv9-CD (Figures 6A and 6B). As expected, mice expressing scFv9 had significantly less RIPA-soluble Aβ42, SDS-soluble Aβ40 and Aβ42, and FA-extracted Aβ40 and Aβ42 compared to controls (Figures 7B–7F). Mice expressing scFv9-CD also had significantly lower levels of SDS-soluble Aβ40 and Aβ42 and FA-soluble Aβ40 and Aβ42 compared to controls (Figures 7B, 7C, 7E, and 7F). However, consistent with our IHC data, CD addition did not improve the effect of scFv9 on amyloid aggregation because there was no difference in Aβ levels between scFv9 and scFv9-CD.

It is interesting to note that the fusion of CD to scFv12 improved the efficacy of scFv12 and further reduced the number of amyloid plaques by 26.2% compared to scFv12 alone. Also, mice expressing scFv12-CD had significantly fewer plaques than controls (Figure 6B). Mice expressing scFv12-CD had significant reductions in SDS-soluble Aβ40 and FA-extracted Aβ40 and Aβ42 compared to controls (Figures 7B, 7C, and 7F). CD fusion to scFv12 reduced the levels of Aβ40 in FA fraction (32.4% as compared to control) (Figure 7C), whereas only a trend to the reduction of SDS-soluble Aβ40 (18.3%) and Aβ42 (12.3%) levels and FA-extracted Aβ42 levels (13.2%) was achieved with scFv12 alone. CD fusion to scFvB11 reduced amyloid plaques by 17.6% compared to scFvB11 alone; however, scFvB11 with or without CD fusion did not significantly affect the plaque count in TgCRND8 mice as compared to controls.

The fusion of scFvB11 to CD did not improve the prevention of scFvB11, and there was no difference in Aβ levels between scFvB11 and scFvB11-CD. These data suggest that the benefit of CD fusion may be limited to scFvs with low affinity.

DISCUSSION

We show that a 126-aa CD derived from C1qTNF3 results in enhanced secretion and multimerization of a variety of fusion partners and enables the facile generation of bifunctional molecules when distinct fusion partners are placed on either end of the CD. Notably, we find that when expressed at high levels throughout the brain of mice by itself, the CD (1) has a negligible systems-level impact as assessed by bulk RNA sequencing, (2) does not alter fear conditioning behavior in APP or non-Tg mice, and (3) does not alter amyloid deposition in APP mice. Pharmacokinetic studies show that

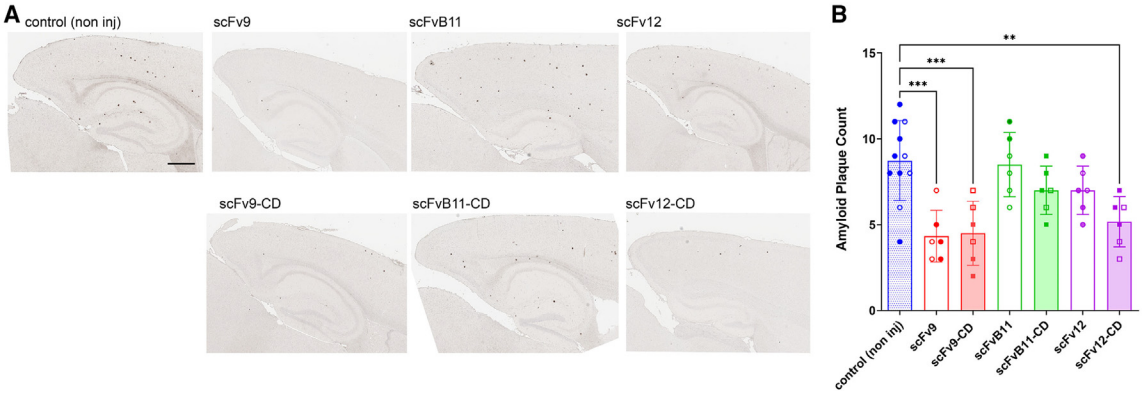

Figure 6. Anti-Aβ scFvs-CD attenuate amyloid aggregation in the brains of TgCRND8 mice following neonatal AAV delivery

(A) Representative images of cortex and hippocampus of TgCRND8 mice injected with rAAV2/1-scFv9, scFv9-CD, scFvB11, scFvB11-CD, scFv12, or scFv12-CD, and non-injected (control) stained with biotinylated anti-Aβ mAb 33.1.1 (anti-Aβ 1–16). Scale bar: 250 μm. (B) Quantification of amyloid plaques immunostained with anti-Aβ mAb 33.1.1-biotin. Data represents scatter dot plot of male (closed circle/square) and female (open circle/square) ± standard error of the mean. n = 11, control; n = 6, scFv9; n = 6, scFv9-CD; n = 6, scFvB11; n = 6, scFvB11-CD; n = 6, scFvB12; n = 6, scFvB12-CD. Plaques were quantified with one-way ANOVA test (**, $p < 0.01$, ***, $p < 0.001$).

the CD fusion modestly increases the half-life of a recombinant scFv injected peripherally into mice, from 0.74 to 1.82 h. Such data suggest that the CD from C1qTNF3 serves as an effective secretory chaperone and multimerization factor that has limited biological impacts on its own.

Proof of concept studies using rAAV vectors to express three different anti-Aβ scFvs either alone or fused to the CD as modulators of amyloid deposition in TgCRND8 mice demonstrated modest effects on the efficacy of a modest affinity anti-Aβ scFv (scFv12), but did not affect the efficacy of a high-affinity anti-Aβ scFv (scFv9). These data are consistent with studies showing that avidity increases due to multimerization are more likely to affect efficacy for low-affinity mAbs,[18–21] and that anti-Aβ scFvs lacking a functionalization domain are unsuccessful in activating a clearance pathway.[22]

Based on studies of C1qTNF family members, CDs derived from these proteins would be expected to result in both trimers and higher-order assemblies of the trimers.[23,24] However, size exclusion chromatography revealed that when fused to the ectodomains of Lag3, the majority of the fusion protein is a dimer, although trimers and larger assemblies are also present. More detailed studies are needed to determine how such variable assembly relates to biological activity. In some cases, further engineering of the fusion protein by altering linker length or position of the fusion partner relative to the CD may be needed to optimize biological activity. In any case, we would note that the increase in secretion of several protein ectodomains could facilitate the generation of rAAV-encoded biotherapeutics simply by acting as a secretory chaperone, because we find that multiple ectodomains that could serve as decoy receptors are only expressed at trace levels unless fused to the CD.

Most recombinant biotherapeutics use fusions to Fc domains, because these provide long half-lives due to FcRn recycling.[22,25] However, unless further engineered, the Fc domains also impart effector fusions that may not be desired. Furthermore, in the context of some gene therapies, whether a focal effect may be desired, the long-lived Fc fusions could lead to the accumulation of circulating species that result in systemic side effects.[26] Although other non-Fc multimerization domains (e.g., COMP48 coiled-coil peptide, domains from human COL18)[19–21,27] have been explored in the context of engineering recombinant biotherapeutics, we were not able to find examples of non-Fc multimerization domain fusion proteins that are expressed *in vivo* using rAAV vectors. Given our current data, use of the current CD or other domains could improve the efficacy of viral-based gene therapies by increasing the secretion and stability of the encoded biotherapeutics and possibly by attenuating their functionality by increasing avidity due to multimerization. Future studies evaluating the current CD and other multimerization domains could dramatically affect both the cost and efficacy of gene therapies that are designed to work in a non–cell-autonomous fashion, simply by increasing the amount of biotherapeutic delivered per vector genome.

Our studies of efficacy of the anti-Aβ scFvs demonstrate that many factors affect anti-Aβ immunotherapies. The high-affinity pan-Aβ scFv9 and scFv9-CD were the most effective biotherapeutics in this study, although the CD had no impact on efficacy. A fibril-selective scFvB11 derived from the aducanumab sequence had limited impact on amyloid loads in this study. Another lower-affinity anti-Aβ scFv12 showed slightly improved efficacy in terms of amyloid reduction when expressed as a CD fusion, but neither the parent scFv nor the CD fusion were as effective as scFv9. Future studies exploring the functionalization of both the scFv9 and the scFv9-CD may provide novel insights that result in the optimization of gene therapy–based intrathecal delivery of anti-Aβ recombinant antibodies. Although selectivity for deposited Aβ, either aggregate selectivity or selectivity against modifications found in deposited Aβ, dramatically improves the efficacy of amyloid reduction for peripheral delivered

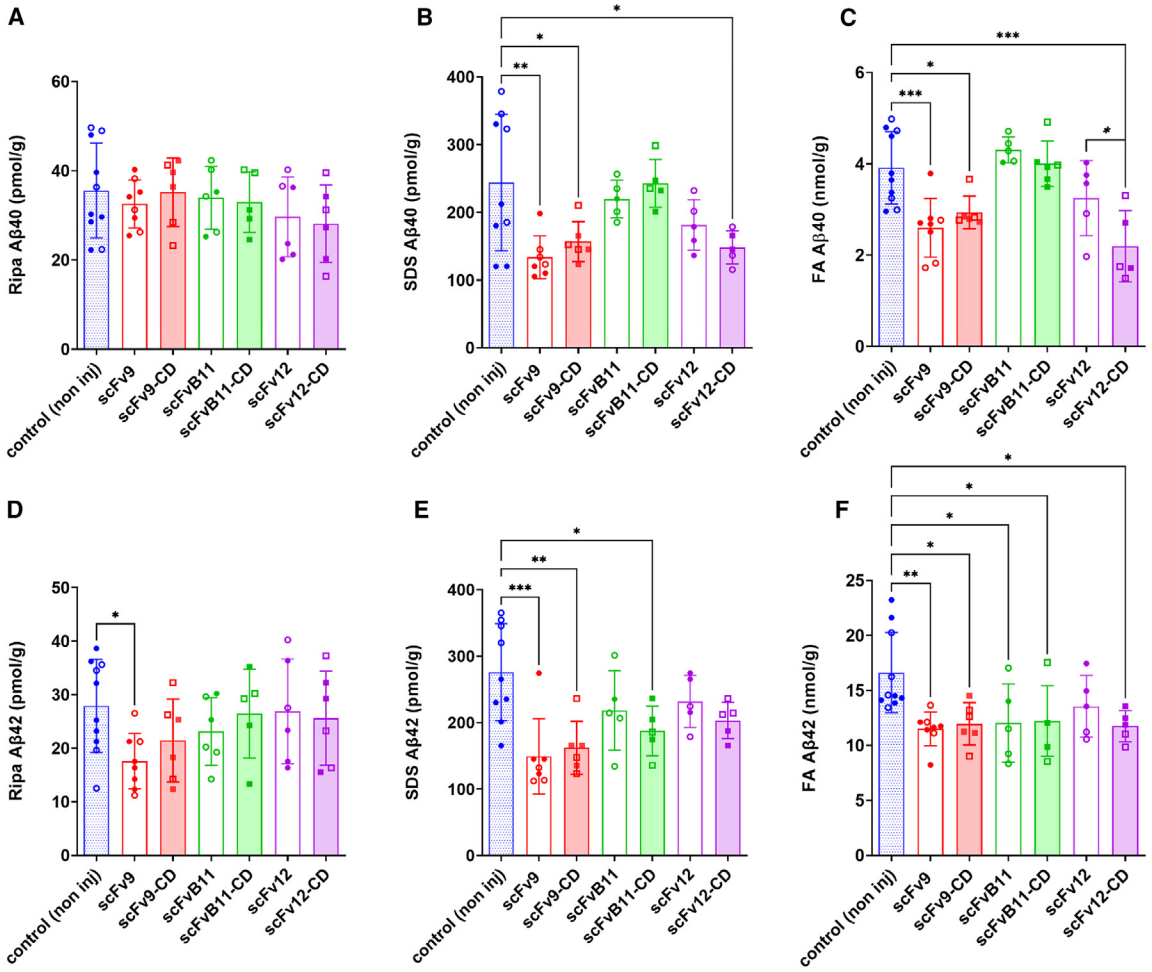

Figure 7. Anti-Aβ scFvs and scFv-CDs prevent accumulation of insoluble amyloid in 3 month old TgCRND8 mice

Mice were intracerebrally injected with rAAV-scFv, scFv-CD or not-injected (control) at P0 and aged 3 months. (A) RIPA extracted Aβ40, (B) 2% SDS extracted Aβ40, (C) 70% formic acid Aβ40, (D) RIPA Aβ42, (E) 2% SDS extracted Aβ42, and (F) 70% formic acid extracted Aβ42. Data plotted as scatter dot plot of male (closed circle/square) and female (open circle/square) ± standard error of the mean. The number of TgCRND8 mice injected with each scFv were as follows: non-injected: n = 10, scFv9: n = 8, scFv9-CD: n = 6, scFvB11: n = 5, scFvB11-CD: n = 5, scFv12: n = 5, scFv12-CD: n = 5. Aβ42 and Aβ40 levels were quantified with corresponding one-way ANOVA and paired comparison test (*, $p < 0.05$; **, $p < 0.01$, ***, $p < 0.001$).

antibodies,[28–31] our current and previous data suggest that binding both aggregates and monomer with high affinity may result in optimal amyloid reduction when the antibody is expressed directly in the brain.

Although we did not test a bifunctional molecule *in vivo*, the CD enables the facile generation of bifunctional biotherapeutics. To significantly affect the course of many diseases, including symptomatic AD, it is likely that a combination of therapeutics will ultimately be needed. Future evaluation of bifunctional biotherapeutics delivered by rAAV may accelerate the identification of therapies that are likely to have a larger impact on disease.

In summary, we have identified a CD that chaperones and stabilizes secreted fusion proteins. The CD itself is small, adaptable, and biologically "inert," and in one case can be shown to improve the efficacy of an anti-Aβ scFv fusion. Given these proof of concept studies, we believe that future studies focusing on this and possibly other domains that can enhance cargo production from gene therapy vectors may help to improve the efficacy of future gene therapies.

MATERIALS AND METHODS

Generation of antibody 2B12

Generation of antibody 2B12 was performed as previously described.[32] Briefly, female BALB/c mice (n = 5) were immunized with synthetic peptides corresponding to the β-secretase cleavage site in APP ($APP^{666–677}$) conjugated to KLH (Genscript, Piscataway, NJ). Protein (100 μg) in 200 μL PBS was emulsified with either 100 μL of Freund's complete adjuvant (first injection; Sigma Aldrich, St. Louis, MO) or Freund's incomplete adjuvant (subsequent injections;

Sigma Aldrich). For the first immunization, mice were injected subcutaneously, IP injections were administered 2 and 4 weeks later. Six weeks following the initial injection, mice were boosted with an IP injection of the peptide in PBS. Three days later, mice were euthanized by CO_2 inhalation, and spleens were harvested using aseptic technique.

Mouse myeloma (Sp2/O-Ag14; ATCC, Manassas, VA) cells were maintained in high glucose (4.5 g/L) DMEM with 10% NCTC 135 Media (Sigma Aldrich), 20% hybridoma grade fetal bovine serum (FBS; Hyclone, Logan, UT), 100 U/mL penicillin, 100 U/mL streptomycin, 2 mM L-glutamine, 0.45 mM pyruvate, 1 mM oxaloacetate, and 0.2 U/mL insulin at 37°C and 8% CO_2, as previously described.[32] Spleens were gently homogenized in 5% FBS/Hank's balanced salt solution (HBSS; Lonza, Walkersville, MD). Cell suspensions were collected and centrifuged to pellet cells. The cell pellets were resuspended in red blood cell lysis buffer (Sigma Aldrich) and diluted with HBSS after 1 min. The cells were then washed twice by centrifuging at 100 × *g* for 10 min and resuspending in HBSS. Sp2/O-Ag14 cells were also washed twice with HBSS. Five million Sp2/O-Ag14 cells were added to 50 million spleen cells and, after centrifuging at 100 × *g* for 10 min onto a culture dish, fusion was induced with 50% polyethylene glycol 1450 (Sigma Aldrich). After washing with HBSS, cells were incubated in Sp2/O-Ag14 media at 37°C with 8% CO_2 overnight. The next day, the cells were gently detached from the plate and distributed into 96-well plates with Sp2/O-Ag14 media/0.5% hybridoma enhancing supplement/sodium hypoxanthine, aminopterin and thymidine selection supplement (both Sigma Aldrich).

All of the hybridoma clones were screened for reactivity to Aβ by ELISA. Immulon 4HBX plates (Thermo Fisher Scientific, Waltham, MA) were coated with 1 μg/mL $APP^{666–677}$ conjugated to ovalbumin, monomeric Aβ4-40, Aβ11-42, Aβ1-28, Aβ1-40, Aβp3-42, or aggregated Aβ1-42 in PBS and blocked with 1% Block Ace in PBS. Media from the hybridomas were applied to plates, which were then incubated at room temperature for 3 h. Next, the plates were washed with PBS and incubated with goat anti-mouse secondary antibody conjugated to horseradish peroxidase (HRP; Jackson ImmunoResearch Laboratories, West Grove, PA) for 1 h at room temperature. Then, the plates were washed and 3,3′,5,5′-tetramethylbenzidine (TMB) substrates (Pierce, Rockford, IL) were applied until color changes were observed. Reactions were then quenched with 85% *o*-phosphoric acid and absorbance was measured at 450 nm. Clones that were positive by ELISA were transferred to larger culture plates as needed.

Tissue array

Mouse tissue microarray was created using the T-Sue Microarray mold kit, 2 mm (Electron Microscopy Sciences, Hatfield, PA) following the manufacturer's instructions. In brief, a recipient paraffin block was created using the supplied silicone mold. Individual tissue samples were punched out of original tissue blocks and transferred to the respective holes in the recipient block. Tissue cores were fixed to the recipient block by incubation at 45°C overnight. The microarray block was resurfaced and 5-μm tissue sections were cut for subsequent experiments.

Cloning and cell culture

cDNAs encoding tandem CD, scFvs, and scFv-CDs were synthesized by Genscript and subcloned into pCDNA3.1 vector and rAAV vector pCTR4 under chicken β-actin promoter. All constructs have FLAG tag (DYKDDDDK) on the -COOH terminal. To overexpress scFvs, 2.7 μg plasmid were transiently transfected into HEK293T cells in a 6-well dish using polyethylenimine. Media was replaced with FBS free Opti-MEM after 18 h of incubation. Cells and conditioned media were collected after another 24 h of incubation. Bis-Tris precast gels (BioRad, Hercules, CA) were used for all SDS-PAGE. Cell lysate, 50 μg, by total protein and 30 μL media of each sample were loaded. Western blot was developed using anti-FLAG M2 mAb and anti-β-actin (Sigma-Aldrich).

Direct ELISA

A number of 96-well plates were coated with 1 μg/mL of either Aβ42 aggregates, prepared as previously described,[33] or monomeric Aβ1-16 in PBS. Media of HEK293Ts expressing scFv9, scFv9-CD, scFvB11, scFvB11-CD, scFv12, or scFv12-CD were incubated in plates for 3 h. Plates were then washed and incubated with HRP conjugated anti-c-myc (1:2,000) for 1 h at room temperature. Plates were washed again and TMB substrate was applied for 10 min. Reaction was stopped with 85% *o*-phosphoric acid and absorbance was measured at 450 nm.

Measurement of scFv in plasma

Biotinylated scFv or scFv-CD (250 μg) was administrated by IP injection into 4-month-old female B6C3F1 mice. Control mice received biotinylated mouse IgG. Cohorts of 4 mice per group were euthanized and plasma was collected at 0, 2, 4, 8, and 24 h after injection. Levels of biotinylated scFv were determined by direct ELISA with Aβ40 (5 μg/well) as capture and NeutrAvidin-HRP as detection. Purified scFv was used as standard. Half-life was calculated by nonlinear regression analysis of one-phase decay.

Animal models and neonatal injections

All of the animal procedures were approved by the Institutional Animal Care and Use Committee in accordance with NIH guidelines. TgCRND8 mice overexpressing APP begin to develop Thioflavin S-positive Aβ amyloid plaques at 3 months of age, with dense-cored plaques at 5 months of age, and impaired performance in a fear-conditioning cognitive task at 6 months of age.[15,34] CRND8 mice were bred in house and housed three to five to a cage and maintained on *ad libitum* food and water with a 12-h light:dark cycle. Intracerebroventricular injections of rAAV2/1 were carried out on day P0 as described previously.[8] Two microliters of rAAV2/1 ($10e^{13}$ genomes per milliliter) encoding CD, scFv9, scFv9-CD, scFvB11, scFvB11-CD, scFv12, or scFv12-CD were administrated bilaterally into each cerebral ventricle.

Mice injected with rAAV encoding CD alone were subjected to contextual fear conditioning paradigm at 6 months of age before

being euthanized. Brains were harvested and one hemibrain was fixed overnight in 4% paraformaldehyde at 4°C for IHC staining and the other hemibrain was snap-frozen in isopentane on dry ice for biochemical analysis.

Mice injected with rAAV encoding scFv9, scFv9-CD, scFvB11, scFvB11-CD, scFv12, or scFv12-CD were aged 3 months and euthanized, brains were harvested, and one hemibrain was fixed overnight in 4% paraformaldehyde at 4°C followed by processing and paraffin embedding for IHC staining. The other hemibrain was snap-frozen in isopentane on dry ice and then stored at −80°C until it was thawed and homogenized for ELISA measurements of Aβ peptide levels.

Contextual fear conditioning

TgCRND8 and NTg littermates, injected with rAAV2/1-CD or PBS as control, were aged 6 months and subjected to contextual fear conditioning as previously described.[15,33] Briefly, mice learn the association between the training chamber, which represents an initially neutral conditional stimulus (CS), and an aversive, brief electric foot shock, unconditional stimulus (US). We have previously established that 0.45 mA electric current elicits robust avoidance response and results in strong freezing response after 2 CS-US pairings.[15] During the training session, mice were allowed to explore the training chamber for 120 s, with a 2-s foot shock immediately following a 30-s tone (80 dB) (day 1). The mice recovered for 60 s and then received another 2 s foot shock following a 30-s tone. For the context test session, on day 3, mice were exposed to the same training context and the percentage of time freezing, during the 300 s, was recorded by an image analysis system (FreezeFrame, Actimetrics, Wilmette, IL). On day 4, mice experienced the tone session, and were placed in a modified chamber (altered inserts and smell). During the first 180 s the mice were allowed to explore the new environment; during the second 180-s period the tone was delivered, and the percentage freezing was recorded. No shock was applied during context or tone session on days 3 and 4.

Histology and IHC

Paraffin sections (5 μm) were used for all histology and IHC studies. Thioflavin S tissue staining methods were performed as previously described.[35] Embedded sections were IHC stained with a biotinylated pan-Aβ antibody Ab5 (1:500; a gift from T.E.G.) or anti-FLAG antibody (Sigma-Aldrich) and developed using the Vectastain Elite ABC Kit (Vector Laboratories, Burlingame, CA) followed with 3,3′-diaminobenzidine substrate (Vector Laboratories) and counterstained with hematoxylin. The slides were scanned by Aperio XT System (Leica Biosystems, Buffalo Grove, IL) and analyzed using the ImageScope program. In brief, at least 3 sections per sample, at least 30 μm apart, were imaged and plaque burden was quantified. For Thioflavin S quantification, one section per sample was used by a blinded observer to calculate the number of cored plaques per area using ImageJ. For 3-month-old mice, the plaque number was calculated by two independent observers.

RNA extraction, sequencing, and analysis

Transcriptome analysis was performed as previously described.[36] Briefly, RNA was extracted from pulverized hemibrains of mice expressing CD or PBS control (n = 4) using TRIzol (Invitrogen, Waltham, MA) followed by a clean-up step using the RNeasy mini extraction kit with on-column DNase treatment (QIAGEN, Hilden, Germany). RNA quality was determined with the Qubit RNA HS assay, and checked via RNA integrity number on an Agilent Bioanalyzer 2100 (Agilent Technologies, Santa Clara, CA) with the eukaryote total RNA nano chip. One microgram of total RNA was used to generate sequencing libraries using the Illumina TruSeq RNA Library Prep kit version 2 (Illumina, San Diego, CA), which enriches for polyA-tailed RNA. Libraries were sequenced on paired-end, 75-bp runs on the Nextseq 500 (Illumina) using a pooling strategy to minimize batch effects from extraction, library preparation, and sequencing.

FASTQ alignment, gene counts, and differential expression analysis

Resulting FASTQ files were aligned against the mouse genome (GRCm39) and GRCm39.107 annotation using STAR[37] to generate BAM files. BAM files were used to generate gene counts using Rsamtools[38] (Bioconductor package) and the summarize overlaps function with the GenomicAlignments package.[39] Differential gene expression analysis was performed with the DESeq2 package using the "DESeq" function with default settings,[40] which fits a generalized linear model for each gene. Subsequent Wald test p values were adjusted for multiple comparisons using the Benjamini-Hochberg method (adjusted p value). Differentially expressed genes were defined as an absolute log2 fold change >1 and an adjusted $p < 0.05$.

Aβ ELISA assay

After tissue harvesting, the left hemisphere was flash-frozen in isopentane. The frozen cortex was sequentially extracted with protease inhibitor cocktail (Roche, Basel, Switzerland) containing RIPA buffer, 2% SDS, and 70% FA as described previously at a concentration of 150 mg/mL.[41] Aβ levels from the 2% SDS- and 70% FA-extracted samples were quantified using end-specific sandwich ELISA.[41] Aβ40 was captured with mAb 13.1.1 (human Aβ35–40 specific; a gift from T.E.G.) and detected by HRP-conjugated mAb 33.1.1 (human Aβ1–16; a gift from T.E.G.). Aβ42 was captured with mAb 2.1.3 (human Aβ35–42 specific; a gift from T.E.G.) and detected by HRP-conjugated mAb 33.1.1 (human Aβ1–16; a gift from T.E.G.). ELISA results were analyzed using SoftMax Pro software (Molecular Devices, San Jose, CA).

Aβ aggregation assay

Aβ42 (Anaspec, Fremont, CA) was pretreated, in brief, solubilized in hexafluoro-2-propanol (Sigma-Aldrich), dried, stored at −20°C, and used within 2 weeks. Reactions were initiated in siliconized Eppendorf tubes by adding 100 μM monomeric Aβ42 with 10 μM CD to the reaction buffer (20 mM Tris-HCl and 150 mM NaCl, pH 8.0) and incubated with shaking at 37°C. Aggregation was monitored by Thioflavin T fluorescence. In brief, at specific time points, an aliquot

of the Aβ reaction mixture was diluted 15-fold in buffer containing 5 mM Thioflavin T and 5 mM Tris HCl, pH 8.0, and fluorescence (excitation 415 nm, emission 487 nm) was measured (FlexStation3; Molecular Devices).[42]

Statistical analysis

Data were analyzed statistically according to the methods specified in each figure legend. Half-life was calculated using nonlinear regression analysis of one-phase decay. The data were compared by ANOVA with post-hoc Tukey's multiple comparisons test. All of the graphs were generated in GraphPad Prism (GraphPad Prism version 9.0 software, La Jolla, CA).

DATA AND CODE AVAILABILITY

The datasets generated and/or analyzed during the current study are available from the corresponding authors on request.

SUPPLEMENTAL INFORMATION

Supplemental information can be found online at https://doi.org/10.1016/j.omtm.2023.101146.

ACKNOWLEDGMENTS

Support was provided by NIH grants R01AG18454 (to T.E.G., Y.L., and B.D.M.), R01AG046139 (to T.E.G.) P50AG047266 (to T.E.G.), and P30AG066506 (to T.E.G.). The graphical abstract was created using BioRender.com. We would like to thank Drs. Dave Borchelt and Guilian Xu for providing mouse tissue for 2B12 antibody testing.

AUTHOR CONTRIBUTIONS

B.D.M., Y.L., and T.E.G. planned the experiments. B.D.M. and B.I.G. generated the 2B12 hybridoma. S.P. provided the tissue sections to test the hybridoma. M.S.G., K.K., and Y.R. performed the molecular cloning and cell culture experiments. B.D.M., K.D., C.C., X.L., and Y.L. performed the animal studies. K.N.M. performed the RNA sequencing. B.D.M., T.E.G., and Y.L. wrote the manuscript.

DECLARATION OF INTERESTS

T.E.G. is a cofounder of Lacerta Therapeutic and Andante Biologics. The other authors declare no competing interests.

REFERENCES

1. Britten-Jones, A.C., Jin, R., Gocuk, S.A., Cichello, E., O'Hare, F., Hickey, D.G., Edwards, T.L., and Ayton, L.N. (2022). The safety and efficacy of gene therapy treatment for monogenic retinal and optic nerve diseases: A systematic review. Genet. Med. *24*, 521–534. https://doi.org/10.1016/j.gim.2021.10.013.

2. Doerfler, P.A., Sharma, A., Porter, J.S., Zheng, Y., Tisdale, J.F., and Weiss, M.J. (2021). Genetic therapies for the first molecular disease. J. Clin. Invest. *131*, e146394. https://doi.org/10.1172/JCI146394.

3. Ferla, R., Dell'Aquila, F., Doria, M., Ferraiuolo, M., Noto, A., Grazioli, F., Ammendola, V., Testa, F., Melillo, P., Iodice, C., et al. (2023). Efficacy, pharmacokinetics, and safety in the mouse and primate retina of dual AAV vectors for Usher syndrome type 1B. Mol. Ther. Methods Clin. Dev. *28*, 396–411. https://doi.org/10.1016/j.omtm.2023.02.002.

4. Jogalekar, M.P., Rajendran, R.L., Khan, F., Dmello, C., Gangadaran, P., and Ahn, B.C. (2022). CAR T-Cell-Based gene therapy for cancers: new perspectives, challenges, and clinical developments. Front. Immunol. *13*, 925985. https://doi.org/10.3389/fimmu.2022.925985.

5. Levy-Mendelovich, S., Walsh, C.E., Schapiro, J.M., Soffer, S., Klang, E., and Kenet, G. (2023). A systematic review of adeno-associated virus gene therapy clinical trials for HIV - A potential solution for patients with haemophilia and HIV? Haemophilia *29*, 784–789. https://doi.org/10.1111/hae.14780.

6. Reilly, A., Chehade, L., Kothary, R., and Curing, S.M.A. (2023). Are we there yet? Gene Ther. *30*, 8–17. https://doi.org/10.1038/s41434-022-00349-y.

7. Ghauri, M.S., and Ou, L. (2023). AAV Engineering for Improving Tropism to the Central Nervous System. Biology *12*, 186. https://doi.org/10.3390/biology12020186.

8. Chakrabarty, P., Jansen-West, K., Beccard, A., Ceballos-Diaz, C., Levites, Y., Verbeeck, C., Zubair, A.C., Dickson, D., Golde, T.E., and Das, P. (2010). Massive gliosis induced by interleukin-6 suppresses Abeta deposition in vivo: evidence against inflammation as a driving force for amyloid deposition. FASEB J. *24*, 548–559. https://doi.org/10.1096/fj.09-141754.

9. Chakrabarty, P., Li, A., Ladd, T.B., Strickland, M.R., Koller, E.J., Burgess, J.D., Funk, C.C., Cruz, P.E., Allen, M., Yaroshenko, M., et al. (2018). TLR5 decoy receptor as a novel anti-amyloid therapeutic for Alzheimer's disease. J. Exp. Med. *215*, 2247–2264. https://doi.org/10.1084/jem.20180484.

10. Levites, Y., Funk, C., Wang, X., Chakrabarty, P., McFarland, K.N., Bramblett, B., O'Neal, V., Liu, X., Ladd, T., Robinson, M., et al. (2021). Modulating innate immune activation states impacts the efficacy of specific Abeta immunotherapy. Mol. Neurodegener. *16*, 32. https://doi.org/10.1186/s13024-021-00453-4.

11. Levites, Y., Jansen, K., Smithson, L.A., Dakin, R., Holloway, V.M., Das, P., and Golde, T.E. (2006). Intracranial adeno-associated virus-mediated delivery of anti-pan amyloid beta, amyloid beta40, and amyloid beta42 single-chain variable fragments attenuates plaque pathology in amyloid precursor protein mice. J. Neurosci. *26*, 11923–11928. https://doi.org/10.1523/JNEUROSCI.2795-06.2006.

12. Levites, Y., O'Nuallain, B., Puligedda, R.D., Ondrejcak, T., Adekar, S.P., Chen, C., Cruz, P.E., Rosario, A.M., Macy, S., Mably, A.J., et al. (2015). A human monoclonal IgG that binds abeta assemblies and diverse amyloids exhibits anti-amyloid activities in vitro and in vivo. J. Neurosci. *35*, 6265–6276. https://doi.org/10.1523/JNEUROSCI.5109-14.2015.

13. Goodwin, M.S., Sinyavskaya, O., Burg, F., O'Neal, V., Ceballos-Diaz, C., Cruz, P.E., Lewis, J., Giasson, B.I., Davies, P., Golde, T.E., and Levites, Y. (2021). Anti-tau scFvs Targeted to the Cytoplasm or Secretory Pathway Variably Modify Pathology and Neurodegenerative Phenotypes. Mol. Ther. *29*, 859–872. https://doi.org/10.1016/j.ymthe.2020.10.007.

14. Fernandez-Funez, P., Zhang, Y., Sanchez-Garcia, J., de Mena, L., Khare, S., Golde, T.E., Levites, Y., and Rincon-Limas, D.E. (2015). Anti-Abeta single-chain variable fragment antibodies exert synergistic neuroprotective activities in Drosophila models of Alzheimer's disease. Hum. Mol. Genet. *24*, 6093–6105. https://doi.org/10.1093/hmg/ddv321.

15. Hanna, A., Iremonger, K., Das, P., Dickson, D., Golde, T., and Janus, C. (2012). Age-related increase in amyloid plaque burden is associated with impairment in conditioned fear memory in CRND8 mouse model of amyloidosis. Alzheimer's Res. Ther. *4*, 21. https://doi.org/10.1186/alzrt124.

16. Sevigny, J., Chiao, P., Bussière, T., Weinreb, P.H., Williams, L., Maier, M., Dunstan, R., Salloway, S., Chen, T., Ling, Y., et al. (2016). The antibody aducanumab reduces Abeta plaques in Alzheimer's disease. Nature *537*, 50–56. https://doi.org/10.1038/nature19323.

17. Thierry Bussiere, P.H.W., Thomas, E., Rhodes, K., Arndt, J., Fang, Q., Dunstan, R.W., and Patel, S. (2014). A METHOD OF REDUCING BRAIN AMYLOID PLAQUES USING ANTI-Aß ANTIBODIES (Wordlwide patent).

18. Asano, R., Koyama, N., Hagiwara, Y., Masakari, Y., Orimo, R., Arai, K., Ogata, H., Furumoto, S., Umetsu, M., and Kumagai, I. (2016). Anti-EGFR scFv tetramer (tetrabody) with a stable monodisperse structure, strong anticancer effect, and a long in vivo half-life. FEBS Open Bio *6*, 594–602. https://doi.org/10.1002/2211-5463.12073.

19. Blanco-Toribio, A., Sainz-Pastor, N., Álvarez-Cienfuegos, A., Merino, N., Cuesta, Á.M., Sánchez-Martín, D., Bonet, J., Santos-Valle, P., Sanz, L., Oliva, B., et al. (2013). Generation and characterization of monospecific and bispecific hexavalent trimerbodies. mAbs *5*, 70–79. https://doi.org/10.4161/mabs.22698.

20. Holler, N., Kataoka, T., Bodmer, J.L., Romero, P., Romero, J., Deperthes, D., Engel, J., Tschopp, J., and Schneider, P. (2000). Development of improved soluble inhibitors of FasL and CD40L based on oligomerized receptors. J. Immunol. Methods *237*, 159–173. https://doi.org/10.1016/s0022-1759(99)00239-2.

21. Zhu, X., Wang, L., Liu, R., Flutter, B., Li, S., Ding, J., Tao, H., Liu, C., Sun, M., and Gao, B. (2010). COMBODY: one-domain antibody multimer with improved avidity. Immunol. Cell Biol. *88*, 667–675. https://doi.org/10.1038/icb.2010.21.

22. Albus, A., Kronimus, Y., Neumann, S., Vidovic, N., Frenzel, A., Kuhn, P., Seifert, M., Ziehm, T., van der Wurp, H., and Dodel, R. (2021). Effects of a Multimerized Recombinant Autoantibody Against Amyloid-beta. Neuroscience *463*, 355–369. https://doi.org/10.1016/j.neuroscience.2021.03.006.

23. Ressl, S., Vu, B.K., Vivona, S., Martinelli, D.C., Südhof, T.C., and Brunger, A.T. (2015). Structures of C1q-like proteins reveal unique features among the C1q/TNF superfamily. Structure *23*, 688–699. https://doi.org/10.1016/j.str.2015.01.019.

24. Xie, Y., Meng, Z., Gao, J., Liu, C., Wang, J., Guo, R., Zhao, J., Lopez, B., Christopher, T., Lee, D., et al. (2021). C1q Complement/Tumor Necrosis Factor-Associated Proteins in Cardiovascular Disease and COVID-19. Proteomes *9*, 12. https://doi.org/10.3390/proteomes9010012.

25. Kelly, V.W., and Sirk, S.J. (2022). Short FcRn-Binding Peptides Enable Salvage and Transcytosis of scFv Antibody Fragments. ACS Chem. Biol. *17*, 404–413. https://doi.org/10.1021/acschembio.1c00862.

26. Suzuki, T., Ishii-Watabe, A., Tada, M., Kobayashi, T., Kanayasu-Toyoda, T., Kawanishi, T., and Yamaguchi, T. (2010). Importance of neonatal FcR in regulating the serum half-life of therapeutic proteins containing the Fc domain of human IgG1: a comparative study of the affinity of monoclonal antibodies and Fc-fusion proteins to human neonatal FcR. J. Immunol. *184*, 1968–1976. https://doi.org/10.4049/jimmunol.0903296.

27. Duchet-Suchaux, M.F., Bertin, A.M., and Menanteau, P.S. (1991). Susceptibility of Chinese Meishan and European large white pigs to enterotoxigenic Escherichia coli strains bearing colonization factor K88, 987P, K99, or F41. Am. J. Vet. Res. *52*, 40–44.

28. Arndt, K.M., Müller, K.M., and Plückthun, A. (1998). Factors influencing the dimer to monomer transition of an antibody single-chain Fv fragment. Biochemistry *37*, 12918–12926. https://doi.org/10.1021/bi9810407.

29. Golde, T.E. (2014). Open questions for Alzheimer's disease immunotherapy. Alzheimer's Res. Ther. *6*, 3. https://doi.org/10.1186/alzrt233.

30. Hudson, P.J., and Kortt, A.A. (1999). High avidity scFv multimers; diabodies and triabodies. J. Immunol. Methods *231*, 177–189. https://doi.org/10.1016/s0022-1759(99)00157-x.

31. van Dyck, C.H. (2018). Anti-Amyloid-beta Monoclonal Antibodies for Alzheimer's Disease: Pitfalls and Promise. Biol. Psychiatry *83*, 311–319. https://doi.org/10.1016/j.biopsych.2017.08.010.

32. Croft, C.L., Moore, B.D., Ran, Y., Chakrabarty, P., Levites, Y., Golde, T.E., and Giasson, B.I. (2018). Novel monoclonal antibodies targeting the microtubule-binding domain of human tau. PLoS One *13*, e0195211. https://doi.org/10.1371/journal.pone.0195211.

33. Moore, B.D., Martin, J., de Mena, L., Sanchez, J., Cruz, P.E., Ceballos-Diaz, C., Ladd, T.B., Ran, Y., Levites, Y., Kukar, T.L., et al. (2018). Short Abeta peptides attenuate Abeta42 toxicity in vivo. J. Exp. Med. *215*, 283–301. https://doi.org/10.1084/jem.20170600.

34. Chishti, M.A., Yang, D.S., Janus, C., Phinney, A.L., Horne, P., Pearson, J., Strome, R., Zuker, N., Loukides, J., French, J., et al. (2001). Early-onset amyloid deposition and cognitive deficits in transgenic mice expressing a double mutant form of amyloid precursor protein 695. J. Biol. Chem. *276*, 21562–21570. https://doi.org/10.1074/jbc.M100710200.

35. Xu, G., Ran, Y., Fromholt, S.E., Fu, C., Yachnis, A.T., Golde, T.E., and Borchelt, D.R. (2015). Murine Abeta over-production produces diffuse and compact Alzheimer-type amyloid deposits. Acta Neuropathol. Commun. *3*, 72. https://doi.org/10.1186/s40478-015-0252-9.

36. McFarland, K.N., Ceballos, C., Rosario, A., Ladd, T., Moore, B., Golde, G., Wang, X., Allen, M., Ertekin-Taner, N., Funk, C.C., et al. (2021). Microglia show differential transcriptomic response to Abeta peptide aggregates ex vivo and in vivo. Life Sci. Alliance *4*, e202101108. https://doi.org/10.26508/lsa.202101108.

37. Dobin, A., Davis, C.A., Schlesinger, F., Drenkow, J., Zaleski, C., Jha, S., Batut, P., Chaisson, M., and Gingeras, T.R. (2013). STAR: ultrafast universal RNA-seq aligner. Bioinformatics *29*, 15–21. https://doi.org/10.1093/bioinformatics/bts635.

38. (2022). Rsamtools: Binary Alignment (BAM), FASTA, Variant Call (BCF), and Tabix File Import. R Package Version 2.12.0. https://bioconductor.org/packages/Rsamtools.

39. Lawrence, M., Huber, W., Pagès, H., Aboyoun, P., Carlson, M., Gentleman, R., Morgan, M.T., and Carey, V.J. (2013). Software for computing and annotating genomic ranges. PLoS Comput. Biol. *9*, e1003118. https://doi.org/10.1371/journal.pcbi.1003118.

40. Love, M.I., Huber, W., and Anders, S. (2014). Moderated estimation of fold change and dispersion for RNA-seq data with DESeq2. Genome Biol. *15*, 550. https://doi.org/10.1186/s13059-014-0550-8.

41. Moore, B.D., Levites, Y., Xu, G., Hampton, H., Adamo, M.F., Croft, C.L., Futch, H.S., Moran, C., Fromholt, S., Janus, C., et al. (2022). Soluble brain homogenates from diverse human and mouse sources preferentially seed diffuse Abeta plaque pathology when injected into newborn mouse hosts. Free Neuropathol. *3*, 3-9. https://doi.org/10.17879/freeneuropathology-2022-3766.

42. Rangachari, V., Moore, B.D., Reed, D.K., Sonoda, L.K., Bridges, A.W., Conboy, E., Hartigan, D., and Rosenberry, T.L. (2007). Amyloid-beta(1-42) rapidly forms protofibrils and oligomers by distinct pathways in low concentrations of sodium dodecylsulfate. Biochemistry *46*, 12451–12462. https://doi.org/10.1021/bi701213s.